A low inflammatory, Langerhans cell-targeted microprojection patch to deliver ovalbumin to the epidermis of mouse skin

A low inflammatory, Langerhans cell-targeted microprojection patch to deliver ovalbumin to the epidermis of mouse skin

Nicole M.D. van der Burg, Alexandra C.I. Depelsenaire, Michael L. Crichton, Paula Kuo, Simon Phipps, Mark A.F. Kendall

PII: S0168-3659(19)30187-7
DOI: https://doi.org/10.1016/j.jconrel.2019.03.027
Reference: COREL 9710

To appear in: *Journal of Controlled Release*

Received date: 3 December 2018
Revised date: 20 February 2019
Accepted date: 29 March 2019

Please cite this article as: N.M.D. van der Burg, A.C.I. Depelsenaire, M.L. Crichton, et al., A low inflammatory, Langerhans cell-targeted microprojection patch to deliver ovalbumin to the epidermis of mouse skin, Journal of Controlled Release, https://doi.org/10.1016/j.jconrel.2019.03.027

A low inflammatory, Langerhans cell-targeted microprojection patch to deliver ovalbumin to the epidermis of mouse skin.

Nicole M.D. van der Burg [a], Alexandra C.I. Depelsenaire [a], Michael L. Crichton [a, 1], Paula Kuo [b], Simon Phipps [c], Mark A.F. Kendall [a, 2]

[a] The Delivery of Drugs and Genes Group (D^2G^2), Australian Institute for Bioengineering and Nanotechnology, University of Queensland, St. Lucia, Queensland, 4072. Australia. Email: nicole.vanderburg@uqconnect.edu.au

[b] The University of Queensland Diamantina Institute, Translational Research Institute, Woolloongabba, Queensland, 4102. Australia.

[c] QIMR Berghofer Medical Research Institute, Herston, Queensland, 4006. Australia.

[1] Presently: School of Engineering and Physical Sciences, Heriot-Watt University, Edinburgh, EH14 4AS. United Kingdom

[2] Presently: The Australian National University, Canberra, Australian Capital Territory, 2600. Australia.

Declarations of interest: MAFK is an inventor on patents licensed to Vaxxas, and founder of Vaxxas, a company developing the Nanopatch ™ for vaccine-delivery applications. Vaxxas does not have a microprojection-based product yet, and the microprojection device presented in this study is not directly related to any microprojection devices that are currently under development at Vaxxas. Both MLC and ACID are inventors on patents licensed to Vaxxas. ACID is now employed by Vaxxas (after the work was conceptualised). The remaining authors state no conflict of interest.

Corresponding author: Prof Mark Kendall (Mark.Kendall@anu.edu.au)

Postal address:

Office of the Vice-Chancellor

The Australian National University

Level 6, 121 Marcus Clarke Street

Canberra ACT 2600

Australia

Abstract

In a low inflammatory skin environment, Langerhans cells (LCs) – but not dermal dendritic cells (dDCs) – contribute to the pivotal process of tolerance induction. Thus LCs are a target for specific-tolerance therapies. LCs reside just below the *stratum corneum*, within the skin's viable epidermis. One way to precisely deliver immunotherapies to LCs while remaining minimally invasive is with a skin delivery device such as a microprojection arrays (MPA). Today's MPAs currently achieve rapid delivery (e.g. within minutes of application), but are focussed primarily at delivery of therapeutics to the dermis, deeper within the skin. Indeed, no MPA currently delivers specifically to the epidermal LCs of mouse skin. Without any convenient, pre-clinical device available, advancement of LC-targeted therapies has been limited. In this study, we designed and tested a novel MPA that delivers ovalbumin to the mouse epidermis (eMPA) while maintaining a low, local inflammatory response (as defined by low erythema after 24 hours). In comparison to available dermal-targeted MPAs (dMPA), only eMPAs with larger projection tip surface areas achieved shallow epidermal penetration at a low application energy. The eMPA characterised here induced significantly less erythema after 24 hours ($p = 0.0004$), less epidermal swelling after 72 hours ($p < 0.0001$) and 52% less epidermal cell death than the dMPA. Despite these differences in skin inflammation, the eMPA and dMPA promoted similar levels of LC migration out of the skin. However, only the eMPA promoted LCs to migrate with a low MHC II expression and in the absence of dDC migration. Implementing this more mouse-appropriate and low-inflammatory eMPA device to deliver potential immunotherapeutics could improve the practicality and cell-specific targeting of such therapeutics in the pre-clinical stage. Leading to more opportunities for LC-targeted therapeutics such as for allergy immunotherapy and asthma.

Keywords: Langerhans cell targeting; Epidermis; Microprojection; Microneedle; Skin delivery; Skin inflammation

Introduction

Many therapies aimed at immune downregulation – such as allergy immunotherapy (AIT) [1], asthma [2], chronic obstructive pulmonary disease [3] and type I diabetes [4] – require tolerance-specific priming via antigen-presenting cells (APCs). One example of an APC able to serve this function is the Langerhans cell (LC) which resides in the skin's viable epidermis. LCs play an important role in both immune defence and immune tolerance for skin infections, inflammations and tumours [5]. During homeostasis, LCs are pre-committed to support the maintenance of tolerance, unlike antigen-primed dermal dendritic cells (dDC) that often induce immunogenicity [6]. Therefore, therapy to boost immune tolerance ideally requires specific delivery of antigens to the LCs within the viable epidermis.

LCs are competent in presenting antigens through both MHC I and MHC II to CD8+ and CD4+ T cells, respectively [5]. They can also induce either specific effector T helper type 2 cell (Th2) [7] or specific regulatory T cell (Treg) responses [8-10]. This ability to induce contradictory T cell responses to the same antigen depends on the local inflammatory environment or adjuvant that the LC is exposed to. That is, high levels of inflammation in the viable epidermis (e.g. removing the *stratum corneum* via tape-stripping) increases the expression of MHC II on LCs that migrate to the draining lymph nodes and bias signalling towards either Th1 or Th2 differentiation [11-14]. Conversely, lower levels of inflammation in the viable epidermis (e.g. topical application of antigen, [13]), favours regulatory pathways including Tregs, and the secretion of interleuken-10 and tumour growth factor-beta [12, 15]. Continuously sampling LCs in the low inflammatory homeostasis state can present antigens to both resident memory Tregs in the skin and circulate to Tregs within the skin draining lymph node [9]. Below the viable epidermis, the dermis contains a large support network for priming of the Th1 and Th2 pathways and thus is better suited for Th1 and Th2 activation-based therapies [7, 16]. Targeting the viable epidermis creates a unique opportunity to enhance specific-Treg responses without activating inflammatory cells within the dermis below.

Targeting and activating LCs in the thin epidermis using the common mouse model is notoriously difficult for several reasons. First, the target site is much thinner than its human counterpart (mouse and human viable epidermal thicknesses, are respectively ~ 20 µm and ~50-100 µm) [17]. Second, small therapeutics do not specifically target the viable epidermis and instead often enter systemic circulation, increasing the chance of an inflammatory

response to the antigen [18, 19]. Third, most of the therapeutics used for AIT are too large to diffuse readily into the skin (i.e. > 500 daltons). Therapies below this size delivered by traditional topical patches can take hours to days of application to deliver the required dose [19, 20].

The unmet challenge is for a range of molecules to effectively bypass the *stratum corneum*, while targeting the viable epidermis, with low-inflammation. To do this, the *stratum corneum* must be either removed, penetrated or hydrated. For example, combining topical patches with devices that removes the *stratum corneum*, such as tape-stripping certainly increases delivery efficiency [21] and LC activation [11]. However, removing the *stratum corneum*, induces local skin inflammation including prolonged skin erythema (over 24 hours) and activating Th2-mediated differentiation [11, 22], rather than tolerance. A review by Larraneta et al. [23] on transdermal devices highlights the importance of reducing local erythema, particularly for repetitive treatments (such as AIT) to maintain patient compliance. Overall, topical patches require an excess of therapeutic drug and long application times making them costly and difficult for patients to comply with but cannot feasibly delivery large sized therapeutics such as AIT quickly without mediating inflammation. Clearly, a more practical delivery device is required for quicker, low inflammatory viable epidermis targeting.

Current research and development efforts are directed at producing transcutaneous devices to deposit therapies either with quick epidermal delivery or alongside a low skin inflammation in mice but not with both characteristics. Quick delivery is defined here as application within 15 minutes and is vitally important for both consistent dosing through the skin and patient compliance [24-26]. Such rapid delivery methods include biolistic microparticle delivery [27], ultrasound-enhanced delivery [28] and ablative micro-fractional laser [29]. While biolistic microparticle delivery and ablative micro-fractional laser can target the viable epidermis within minutes, they are also highly inflammatory (e.g. [30]) relative to the lower-inflammatory hydration chamber device called Viaskin® [31]. Viaskin® relies on actively enhancing diffusion through the stratum corneum but remains slow to delivery. Indeed, no mouse-based viable epidermis device is available to both deliver quickly whilst inducing only a low level of skin inflammation. A class of device with the potential to meet this need is the microprojection array (MPA), which make up part of the microneedle field.

MPAs are defined here as patches with an array of solid or dissolvable projections no taller 1 mm high each. The primary interest for MPA research and development in the last two decades has been on vaccination. MPAs are a more practical device than other skin delivery devices and is more tolerated by medical staff and patients alike [32]. Additionally, their micro wound delivery mechanism elicits activation of the immune response, mitigating the need for additional chemical adjuvants [33]. Most MPAs tested on human skin have penetrated into the epidermis and dermis, though some may indicate epidermal-only penetration is achievable with current conical-projection designs since the human epidermis is much thicker than mice, though no specific penetration measurements were reported [34]. However, there have been no pre-clinical mouse immune tests with MPAs that successfully penetrate only into the epidermis, causing a gap the translation of delivering therapeutics to the epidermis between mice and human trials. Dermal-targeted MPAs (dMPAs) have a broad design range to induce a variety of skin inflammation responses. For example, a dMPA of with five projections each 750 μm (H) applied to mouse skin by hand resulted in erythema that cleared within 24 hours [35]. Using a higher density of projections such as dMPAs of 21,000 projections/cm^2, ranging in length of 40-190 μm applied to mouse skin by a spring loaded applicator resulted in persistent erythema up to 48 hours [36]. Applicators can maintain a consistent MPA application into the skin, but can impart additional energy into the skin and increase the inflammatory skin response. Indeed, dMPAs have been designed and used in many shapes, densities and materials and have been extensively reviewed elsewhere [37]. An MPA to specifically target the mouse epidermis, with low inflammation, however, is yet to be reported.

Here, we hypothesised that an epidermal-targeted MPA (eMPA) with low, local inflammatory characteristics would specifically target coated therapeutics to LCs without enhancing an inflammatory response. To test this hypothesis, we first designed and tested the delivery parameters of an eMPA for mice. We then characterised the local skin inflammatory response of the application area of the eMPAs. Thirdly, we assessed the effect of eMPA application on LC migration. We found that in order to combine epidermal delivery with a low inflammatory application energy, the eMPA projection design required a higher tip surface area (relative to a dMPA). This eMPA elicited low epidermal inflammation and, concurrently, increased LC activation with low MHC II expression without inducing dermal dendritic cell (dDC) migration. These findings of LC-activating, low-inflammatory mouse

eMPAs could have wide-reaching implications, providing a more practical delivery platform to deliver tolerant based therapeutics in a pre-clinical model.

Methods

Animals

Female 6-8 week old BALB/c mice were obtained from the Australian Research Council (Perth, W.A.). Animals were maintained in accordance with The University of Queensland Animal Ethics guidelines. All experimental procedures were approved under ethics AIBN 556/12, AIBN 042/16 and AIBN 043/16. When applying MPAs, animals were anaesthetised by intraperitoneal injection with a Ketamine (50 mg/kg) and Xylazil (10mg/kg) mix (both Troy laboratories, Smithfield, Australia) and its action reversed with atipamezole (Antisedan; Pfizer, Australia) diluted 1:10 in Phosphate Buffered Solution (PBS). Twenty-four hours prior to MPA application, dorsal and flank hair was removed using electric hair clippers (Wahl, Stirling IL, USA), then chemically removed with a depilatory cream (Nair, Church & Dwight, Trenton NJ, USA). After 24 hours, histological analysis of the Nair skin compared to naïve skin found that Nair did not affect the skins thickness or cellular infiltration as previously reported [38]. All injections were performed using a 31G needle.

Microprojection array fabrication

Silicon MPA fabrication

Silicon MPAs were fabricated as previously described [39] with assistance from the Australian National Fabrication Facility Queensland Node. The area of the silicon wafer within 90% consistency was isolated and used for moulding ('silicon master'). Projection designs included conical-shaped, 207 µm ± 5 µm tall projections at 10,000 (10k) projections/cm^2 (p/cm^2), herein referred to as conical-MPA (Figure 1A) or slit shaped, 110 µm ± 3 µm tall projections at 7k p/cm^2 (Figure 1B), herein referred to as slit-MPA. A similar conical-MPA design was first reported in Depelsenaire et al. [33] (previously named 'Nanopatch') and slit-MPA design in Crichton et al. [40] (previously named 'Transdermal patch'). Silicon MPAs were imaged using secondary scanning electron microscopic (SEM) imaging (Hitachi, SU3500).

Polycarbonate hot embossing of MPAs

To fabricate polycarbonate MPAs, a polydimethylsiloxane (PDMS) mould was made by pouring a 1:12 Sylgard-184 mixture over a salinized silicon master (using trichloro(octadecyl)silane, Sigma Aldrich 104817). Polycarbonate projections were hot embossed at 3,500 N as per Yeow et al. [39] with the following stacking: bottom platen, 1 mm polycarbonate foil, PDMS mould, top platen, 1 mm-thick graphite pad. Repeated use of

PDMS mould (over 5 repeats) required 3,600 – 4,000 N pressure to continue producing consistent projections. Conical-MPA projections became 190 ± 4.7 µm tall (Figure 1C) and slit-MPA projections became 95 ± 2.4 µm tall (Figure 1D). Finally, polycarbonate MPAs were diced to 4 x 4 mm squares using a 0.1 mm nickel blade EVG dicer and treated with oxygen plasma prior to formulation coating to increase wettability. MPAs with a surface area of 16 mm^2 had 1,600 projections per Conical-MPA and 1120 projections per slit-MPA. Polycarbonate MPAs were splutter coated with iridium then imaged using back-scatter scanning electron microscopic (BS-SEM) imaging (Hitachi, SU3500). Surface area of projections within the epidermis was calculated by measuring 10-20 projections from SEM images. The height (H) used was the average depth of the epidermis calculated in this report (26 µm). The following equations were used to calculate the average surface area of one projection then multiplied by the number of projections per MPA.

- Lateral surface area of a cylinder for conical: $A = 2\pi r26 \times 1600 \text{ projections } (\mu m^2)$
- Surface area for slit (i.e. 2 × trapezoid + 2 × equilateral triangle surface areas): $\left(2\left(\left(\frac{27+W}{2}\right)H\right)\right) + \left(2\left(\frac{H*D}{2}\right)\right) \times 1120 \text{ projections } (\mu m^2)$

Therapeutic coating of microprojection arrays

Polycarbonate MPAs were coated as previously described [41]with a final concentration of 100 mM PBS and 1% methylcellulose (HG 60). Either ovalbumin (OVA, Sigma, Grade V, 98%, filtered through 0.22 µm) diluted in PBS or PBS alone (placebo) was added to the coating solution. A ^{14}C-OVA-based coating assay was used to calculate delivered dose [42]. The mean delivery efficiency of each condition (see SUPP 1) was measured and the OVA concentration was adjusted in each formulation to ensure each OVA-coated MPA delivered 0.1 µg of OVA while the concentration of the excipients stayed the same for each (e.g. an MPA condition with a delivery efficiency of 10% would be coated with 1 µg OVA). To coat the formulations, MPAs were fixed in place on a coating rig with a vacuum before formulation was dispensed. The rotating MPA was dried with a jet stream of nitrogen gas at 23 °C. Consistent coating was confirmed with BS-SEM (Hitachi, SU3500) (SUPP 2).

Application of microprojection arrays to skin

To prepare the skin for application, a fold of flank skin was extended and fixed as described in Coffey et al. [43]. The skin was not over stretched and was applied to in its natural tension (Figure 1E insert). A push-through spring loaded applicator was used to accelerate the MPA

over 1 - 2 mm of space before contacting the skin fold as previously described [44]. The MPA was removed after 2 minutes, after which the desired dose of formulation was deposited in the skin, as confirmed previously [41]. A maximum of eight applications could be applied per mouse without applications overlapping (Figure *1*E). The 36 gram plunger of the push-through applicator was loaded to deliver MPAs with application velocities (and energies) of 0.9 m/s (15 mJ), 1.3 m/s (30 mJ), 1.8 m/s (60 mJ), 2.3 m/s (100 mJ) or 3.1 m/s (170 mJ).

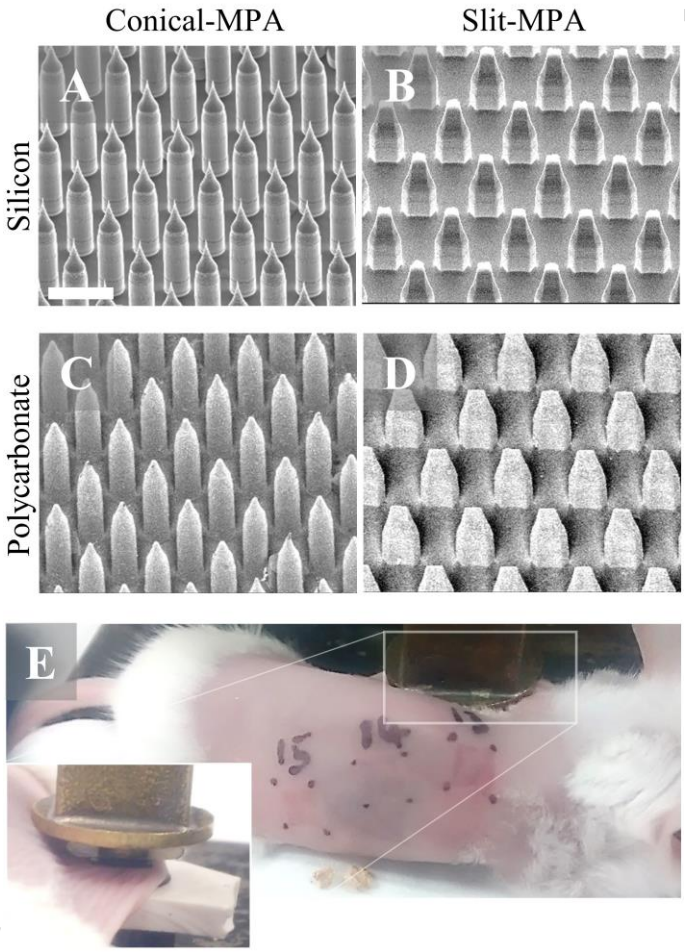

Figure 1: **Representative images of MPA design and application using a mouse model.** Secondary SEM image of silicon masters of (A) conical-MPA projections and (B) slit-MPA projections. BS-SEM image of polycarbonate moulded MPAs coated in iridium of (C) conical-MPA and (D) slit-MPA. Scale bar for A-D is 100 µm. (E) Photograph of flank positioning during MPA application on a mouse, insert depicts close up of 4 x 4 mm MPA applied to flank skin fold with push-through applicator plunger visible.

Measurement of penetration depth and epidermal displacement

Fluorescent penetration tracks were measured using histology to quantify skin penetration depth. Polycarbonate MPAs were coated with an OVA-based formulation including 0.05% yellow-green 200 nm FluoSpheres (F8811, Thermo Fischer scientific, USA), applied to mouse skin for 2 minutes and penetration depth analysed as previously published [45]. A minimum of three 20 µm thick cyro-sections from n = 3 mice were imaged at 20x and analysed using the Zeiss confocal microscope LSM510 with Zen software 2010. Only MPA conditions that resulted in visual fluorescent penetration were imaged for quantification.

Assessment of epidermal inflammation

To assess skin erythema, OVA-coated eMPA and dMPAs were applied to mouse flanks and then imaged at t = 0, t = 24 and t = 72 h after application. Images were scored using the Draize Index as per [46, 47]. Representative images for each condition can be found in SUPP 3. Viable epidermal-specific swelling was quantified after eMPA, dMPA or a 20 µl i.d (31 G) injection. Applied skin was excised (~2 mm deep) at t = 24 or t = 72 h, fixed (10% Neutral Buffered Formalin for 2 h), embedded in paraffin and sectioned to 10 µm thick. Sections were stained with heamatoxylin (HHS32, Sigma-Aldrich) and eosin (E4009, Sigma-Aldrich) (H&E) and mounted under dibutylphthalate polystyrene xylene, DPX (3197, Ajax, Thermo Fischer, USA). Stained sections were imaged with an Aperio slide scanner microscope and epidermal and dermal thicknesses were measured at 20x using ImageScope software. The thickness of each application condition was compared to naïve skin of three mice. Note here that skin thickness in paraffin embedded sections were consistently thinner than cyro-sections and so comparisons were made to naïve skin within respective mediums.

Discrimination of viable / non-viable cells via microscopy

To discriminate between live and dead cells, the viability dyes Acridine Orange and Ethidium Bromide were used as described elsewhere (e.g. [30, 33]), with the following adaptions for thicker flank skin compared to previously used ear skin. Briefly, OVA-coated and applied eMPAs and dMPAs or intradermal injection (i.d.) applied flank areas were excised immediately after euthanasia with at least 3 mm excess border around the site. Skin was submerged under a mix of Acridine Orange (15 µg/ml) and Ethidium Bromide (50 µg/ml) in PBS and incubated at 37 °C for 1.5 hr. MPA-applied skin was imaged (20x, 40-70 µm deep at 1 µm z-stack intervals) using the Zeiss LSM510 confocal microscope. Ethidium Bromide positive dead cells were quantified using Imaris software (assuming a 5.18 µm cell diameter).

The number of dead cells in an MPA contact area of 16 mm^2 were extrapolated from 3-4 3D-images (1.095-1.460 mm^2) of each application repeat.

Flow cytometry

Flow cytometry was used to identify skin APCs migrating to the inguinal draining lymph node (dLN) after eMPA or dMPA application compared to naïve dLNs. Total numbers of DCs, and LC and dDC subsets were quantified per flow sample of each dLN at either t = 24, 48 or 72 h after a PBS MPA (left dLN) and a 0.1 µg OVA MPA (right dLN) application. dLNs were processed individually, however, based on Kool et al. [48], an ipsilateral cross over of cell migration from skin application can make up to 20% of the opposite dLNs cell content. dLN were digested with collagenase D (1 mg/mL) and DNase I (0.2 mg/mL) for 30 minutes at 37°C. dLNS were individually homogenised, washed through a 0.22 µm strainer and resuspended in sterile 0.1% foetal calf serum (in PBS) dilution buffer. Aqua (cat:L34966, Thermo Fisher) was used for live/dead differentiation and anti-mouse monoclonal antibody to CD16/32 (2.4G2, cat:553142, BD Pharmingen) blocked exposed Fc sites. Then anti-mouse monocolonal antibodies against CD11c (N418, cat:25-0114-82, eBioscience), CD11b (M1/70, cat:101226, BioLegend), CD326 (EpCAM) (G8.8, cat:118214, BioLegend), MHC II (M5/114.15.2, cat11-5321.85, eBioscience) were added, and associated isotypes were used for controls (spleen). Cells were incubated, washed and analysed as previously published [49]. Cells were acquired using the Gallios cytometer and analysed with Kaluza software.

Statistics

Statistics were performed in Graphpad Prism (version 6 or 7 for Windows; GraphPad 140 Software, La Jolla, CA) using unpaired t-tests assuming Gaussian distribution between either naïve or sensitised and treated groups. Statistical differences between a number of comparable groups was assessed using a one-way ANOVA (Supplementary figures only). P-values of ≤ 0.05 were considered as significant. All values are expressed as mean ± standard deviation (SD) unless otherwise stated. All groups that resulted in a significant ($p \leq 0.05$) difference with another group within the graph was denoted with an asterisks equal to the significance grouping: *$p \leq 0.05$, **$p \leq 0.01$, *** $p \leq 0.001$, **** $p \leq 0.0001$. All non-significant results ($p > 0.05$) have no symbol in graphs.

Results

Slit-shaped polycarbonate MPAs primarily deliver coating to the epidermis

To establish MPAs for epidermal targeting, we first manufactured MPAs in polycarbonate material. As reported previously by Yeow et al. [39], polycarbonate is a well-suited material for MPA fabrication including relatively low cost, high modulus and high impact strength. The hot embossing procedure of the same silicon master also allows for easy replication of consistent MPA projections unlike the dry etching process of silicon MPA fabrication. Here, hot embossing of high-density projections required optimisation of the PDMS mould to increase flexibility. Here, we found a ratio of 1:12 curing agent to PDMS was better suited (i.e. fewer breakages) for repeated, high-pressure hot embossing (SUPP 4), which differed from the recommended 1:10 ratio. By optimising the PDMS mould and hot embossing procedure, we were able to reproduce silicon master MPAs into polycarbonate MPAs using the same mould multiple times. The polycarbonate projections retained the same base width but were 10-15% (20 µm) shorter than their silicon masters (compare Figure *1*A to C and B to D). Polycarbonate slit-MPA tips increased in width (see Figure 2A) from an average of 0.71 ± 0.15 µm to 2.16 ± 0.35 µm (Figure 2B) similar to Yeow et al. [39]. Figure 2C indicates that conical-MPA or slit-MPAs that penetrate 15 µm equate to the surface area of the bevel of a 27 – 31G needle used for intradermal injections into mouse skin. The polycarbonate projections were significantly blunter than the master but maintained > 85% projection length and 100% projection width and depth of the master projections.

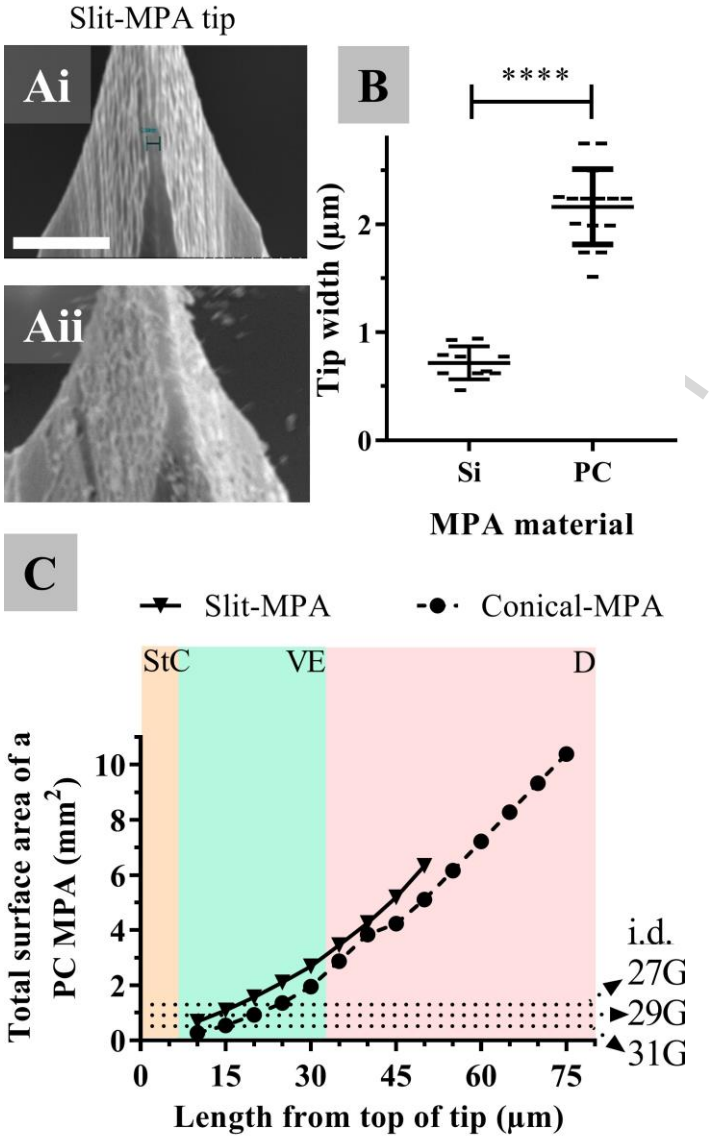

Figure 2: Surface area of polycarbonate projections. (A) BS-SEM image of slit-MPA tip from (i) silicon or (ii) iridium-coated polycarbonate MPA, scale bar is 10 µm. (B) Plot of tip width quantification for silicon, 'Si', and polycarbonate, 'PC', slit-MPA projections. (C) Calculated total projection surface area of a polycarbonate MPA (y-axis) that would be present in the skin depending on the depth of penetration (x-axis) including background shading of average depth of *stratum corneum*, 'StC', viable epidermis, 'VE', and dermis, 'D'. Plot includes surface area of intradermal (i.d.) affected area using a 27, 29 and 31G needle assuming only bevel of needle is inserted.

To target the epidermis specifically, polycarbonate conical- and slit-MPAs were applied at a range of application energies (15, 30, 60 or 100 mJ) and BS-SEM confirmed consistent

removal of coating (Figure 3A). As BS-SEM is not a reliable method to assess penetration depth due to skins viscoelasticity during application, penetration was assessed by histological analysis of applied skin sections using fluorescently coated MPAs (Figure 3B). As the mouse epidermis (StC + viable epidermis) in the flank averages 26.5 ± 4.6 µm thick (Figure 3C), we initially tested shorter (75 µm), conical-MPAs. The combination of short and blunt projections did not penetrate the skin at a low application energy (data not shown), unlike similar short (40 µm) but sharp conical-MPAs reported to penetrate mouse flank skin [36]. On the contrary, Figure 3D shows penetration of 190 µm long conical-MPAs deposited coating beyond the epidermis at the lowest application energy (15 mJ, 31.5 ± 9.0 µm). However, the slit-MPA consistently delivered coating into the viable epidermis (15.7 ± 9.2 µm) using a 30 mJ application energy. Based on these observations, we defined the slit-MPA applied at 30 mJ as the 'eMPA' and the conical-MPA applied at 100 mJ as the 'dMPA' for comparison (which delivered to a depth of 75.2 ± 26.3 µm, Figure 3D). Figure 3E represents the total projection surface area / volume within the skin strata based on the average depth of penetration for both eMPA and dMPA given in Figure 3D. Once applied, the total surface area of the eMPA and dMPA projections is 1.09 ± 0.64 mm^2 and 5.22 mm^2 within the viable epidermis respectively (Figure 3F, left). This equates to a displacement volume of 0.002 ± 0.001 mm^3 (0.47%) or 0.055 mm^3 (13.32%) within the 0.416 mm^3 (i.e. 4 x 4 x 0.025 mm) volume of the viable epidermis respectively (Figure 3F, right). Although an intradermal injection bevel insertion affected a smaller surface area in the epidermis (0.869 mm^2, based on a 10 degree insertion) than the MPAs, it displaced an order of magnitude more volume (0.032 mm^2) than the eMPA and an order of magnitude less than the dMPA. Plotting the epidermal surface area multiplied by the application energy (mm^2 × mJ) highlights the log10 correlation between the three devices (SUPP 5). Note here that the energy of the i.d. injection was approximated to 0.83 mJ based on previously published insertion energies [50]. Additionally, the total tip surface area of the eMPA (0.062 ± 0.01 mm^2) was 1.5-fold higher than dMPA (0.041 ± 0.01 mm^2) (Figure 3G). By normalising the energy of application to the total tip surface area, the eMPA was applied at 5x less energy per mm^2 than the dMPA (483 and 2439 mJ / mm^2, respectively). Taken together, these results provide evidence that slit-MPAs, with significantly higher tip surface areas than conical-MPAs, are better suited for epidermal only delivery using low application energies. By contrast, even when using the lowest application energy tested, higher density conical-MPAs deliver beyond the viable epidermis into the dermis and therefore were deemed not suitable for epidermal only delivery.

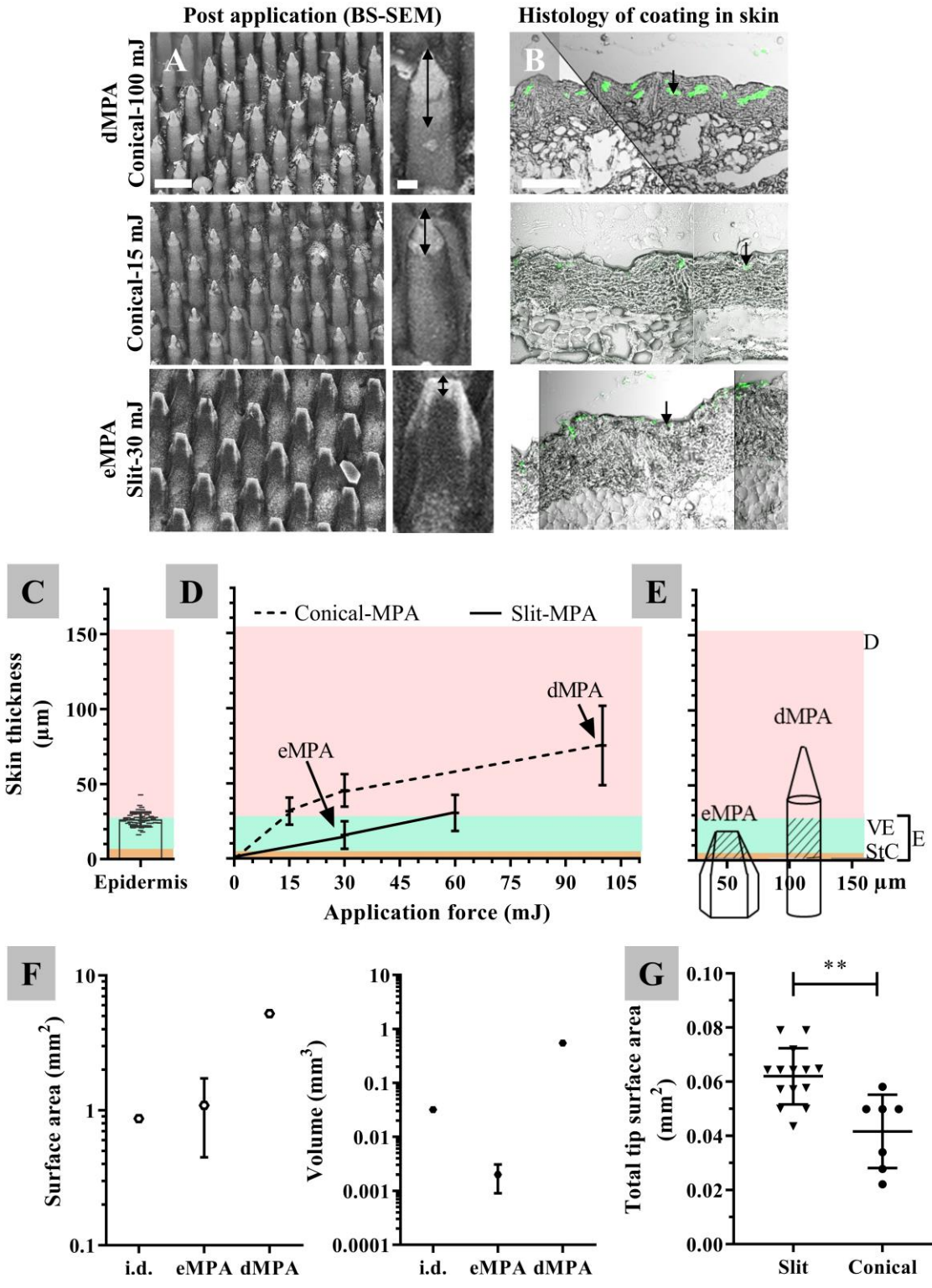

Figure 3: Slit-MPAs applied at 30 mJ deposited coating to the epidermis of mouse skin. (A) BS- SEM of applied OVA-coated MPA per projection shape and application energy. Images indicate areas of coating (dark) and removed coating (light), inset include black arrow

of length of coating removed, scale bars: 100 µm, 10 µm inset. (B) Confocal images of 20 µm sections of green FluoSpheres delivered by MPAs into mouse flank skin, scale bar: 200 µm. Arrow indicates one of the projection tracks per image (arrow 75 µm long). (C) Depth of the epidermis using cryo preserved sections of naïve skin. (D) Skin penetration depth measurements of MPA projections from n = 3 mice, totalling n = 41-117 measurements, mean ± SD. (E) An outline of the average depth of eMPA and dMPA penetration into the skin, based on Figure 2D, shading indicates the area of the projection within epidermis. (C-E) The average skin strata thicknesses: orange ('StC' *stratum coreum*), green ('VE' viable epidermis) and pink ('D', dermis), where StC + viable epidermis together make up the epidermis, 'E'. (F) Calculated epidermal surface area (left) and volume displaced (right) of an applied 31G needle bevel (i.d.), eMPA or dMPA. eMPA includes error based on penetration depth while dMPA epidermal area and volume does not differ within the SD of penetration. (G) Total surface area of polycarbonate tips for conical-MPA or slit-MPA, n = 7 and 14 projection tip measurements respectively.

Application of eMPAs resulted in a lower inflammatory response than dMPAs

Skin inflammation of the applied area was assessed by erythema, epidermal thickness and cell viability quantification. Progression of erythema was captured by photographic images taken at 5 minutes (t = 0 h), t = 24 h and t = 72 h after application (SUPP 3). Photo images were then scored using Draize score index for erythema (Figure 4A). Immediately after application, the application site of MPA or i.d. bleb was clearly visible (SUPP 3). The eMPA induced significantly less erythema than the dMPA at t = 0 h ($p = 0.0002$), t = 24 h ($p = 0.0004$) and t = 72 h ($p = 0.025$) (Figure 4B). All i.d. injections received a Draize score of zero.

Next, we assessed the effect of the eMPA application alone (PBS coating) on the swelling of the viable epidermis using H&E-stained histology sections (Figure 5A). The thickness of the naïve viable epidermis averaged 15.9 ± 5.0 µm and the thickness of the dermis averaged 178.4 ± 29.6 µm. The dermis became thinner 24 h after each application (dMPA $p < 0.0001$, eMPA $p = 0.007$, i.d. $p < 0.0001$, SUPP 6). Twenty-four hours after both the dMPA ($p < 0.0001$, 19.8 ± 5.4 µm) and eMPA application ($p = 0.002$, 18.6 ± 6.1 µm) the viable epidermis increased in thickness (Figure 5B). Concurrently, the thickness of the viable epidermis after i.d. injection reduced slightly at 24 h ($p = 0.038$, 13.4 ± 7.9 µm) but had returned to naïve thickness by 72 h (15.4 ± 6.2 µm). By 72 h, the eMPA viable epidermis

thickening had dissipated (14.1 ± 6.2 µm) while the dMPA maintained an inflamed viable epidermis (20.36 ± 6.8 µm). These results show that the eMPA induces significantly less local inflammation in the viable epidermis than the dermal-targeted device.

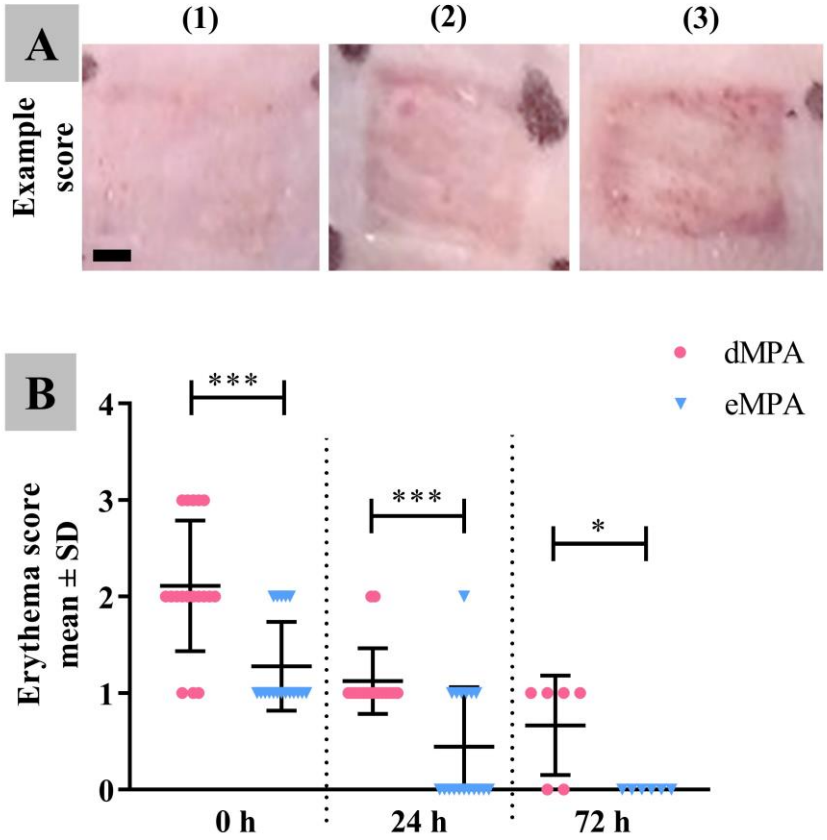

Figure 4: eMPA resulted in lower erythema than dMPA at t = 0, 24 and 72 h. (A) Representative images of MPA-applied flank skin that scored (left to right), 1, 2 and 3 using Draize scoring, scale bar: 1 mm. (B) Plot of Draize score of application sites t = 0, 24 and 72 h after dMPA or eMPA application, n = 3 – 9 mice and n = 6 – 18 applications.

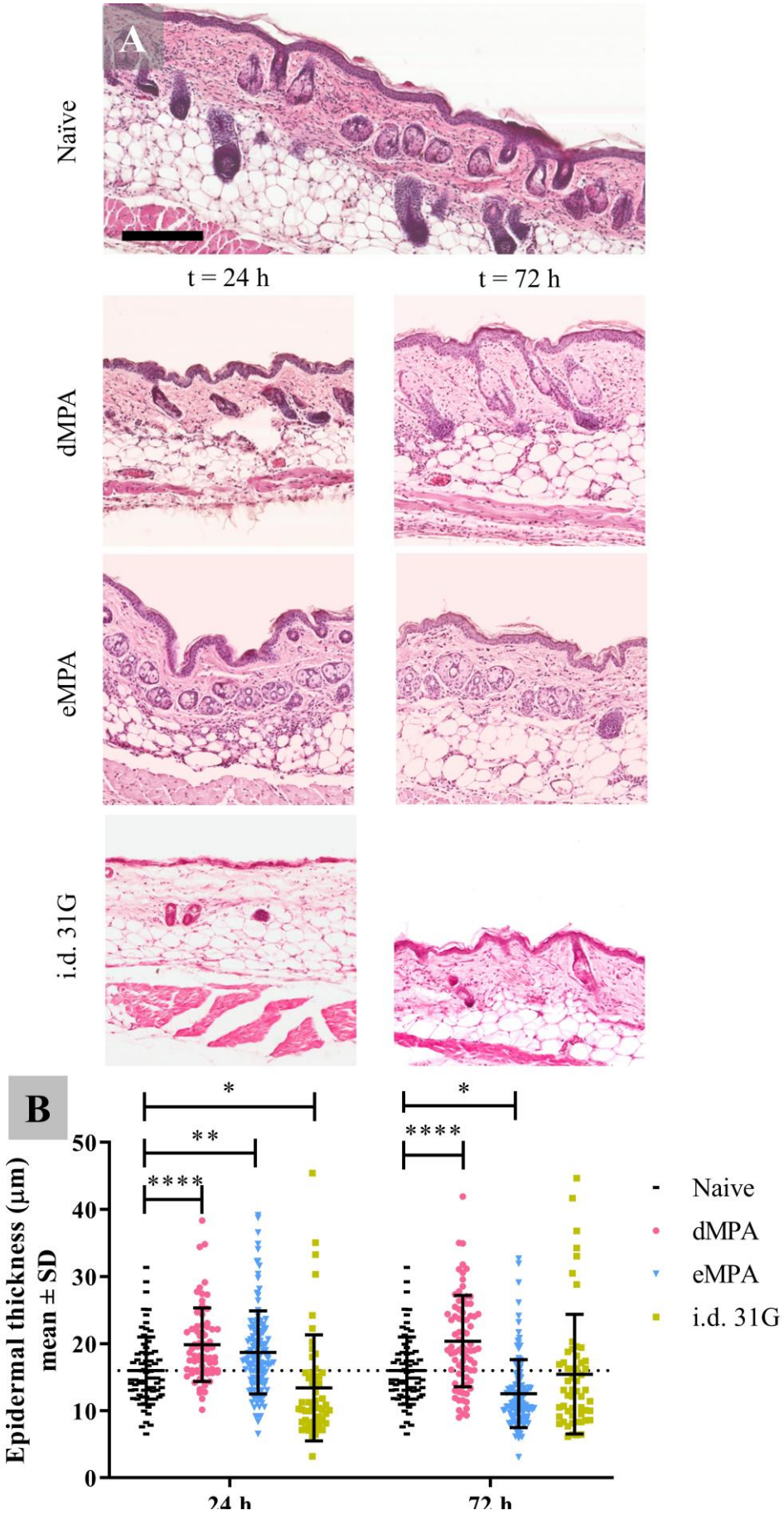
A
Naïve
t = 24 h
t = 72 h
dMPA
eMPA
i.d. 31G
B
Epidermal thickness (µm)
mean ± SD
50
40
30
20
10
0
*
**
****
*
****
24 h
72 h
Naive
dMPA
eMPA
i.d. 31G

Figure 5: eMPA evoked less swelling of the viable epidermis than dMPA. Swelling of the epidermis and dermis 24 h and 72 h post application of placebo formulation/injection. (A) Representative image of H&E-stained flank skin sections (10 µm) of naïve, 24 h post-dMPA, 72 h post-dMPA, 24 h post-eMPA, 72 h post-eMPA, 24 h post-20 µl i.d. and 72 h post-20 µl i.d, scale bar: 200 µm. (B) Epidermal skin thickness measured from H&E-stained sections of n = 3 mice and n = 54-179 measurements per condition, dotted line indicates mean of naive measurements (n = 3 mice with n = 4 sections each).

The physical application of devices to the skin, such as tattoo needles [51] and the Nanopatch™ (a high-density dMPA applied to the skin to deliver vaccine [33]) are known to induce localised cell death. As cell death is associated with an increased pro-inflammatory response [52-54], we sought to quantify the effect of the MPAs used here by quantifying non-viable cells in 16 mm^2 of the epidermis (Figure 6). Individual non-viable (dead) cells could only be quantified immediately after application (t = 0 h) by confocal microscopy. Even though Draize scores were low (typically 0-1) for eMPA and not present for i.d. at t = 24 h, images taken at t = 24 h and t = 72 h confirmed the presence of non-viable cells (Figure 6A and B). At t = 24 h, the cell death appears to have spread further than at t = 0 h which may be due to either easier accessibility of the ethidium bromide dye staining disintegrating cells at each site or additional cell death such as necroptosis [55]. At t = 0 h the dMPA had visually induced the highest proportion of dead cells that seemed to lyse similar to the eMPA at t = 24 h (Figure 6C). This was reflected in Figure 6D, where quantification of dead cells at t = 0 h resulted in a clear trend of increasing number of dead cells from i.d. < eMPA < dMPA. Plotting the total number of dead cells against the epidermal mm^2 × mJ indicated that mm^2 × mJ on a log10 scale correlated with the number of dead cells. Overall, the eMPA resulted in significantly more total cell death (9614 ± 1359, p=0.0005) within the epidermis than the i.d. injection (1227 ± 904), while the dMPA (18297 ± 1271) resulted in the most epidermal cell death (i.d. $p < 0.0001$, eMPA $p = 0.0013$, Figure 6D). Although it is important to note that not all non-viable cells would have been accounted for during the larger volumes displaced in the epidermis by the i.d. and dMPA – as apparent by the black spaces in the images (Figure 6, t = 0 h). This analysis further supports that the eMPA application to skin results in a relatively low local skin inflammation. Additionally, the cell death imaging specifically highlights the prolonged effect microprojection skin penetration has on the epidermal cells (i.e. cell death still visible up to 72 h, despite Draize scores of zero).

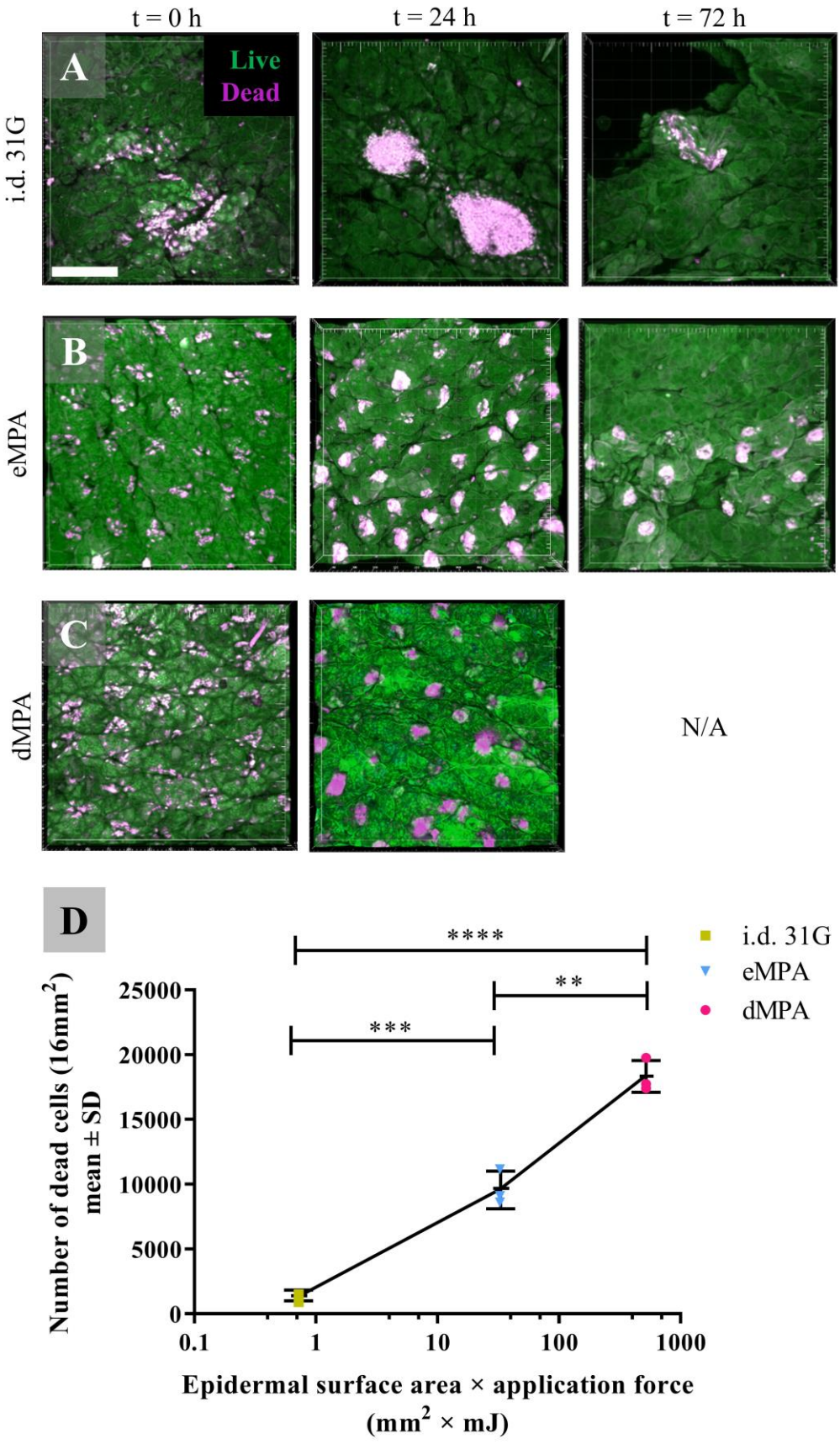

Figure 6: Application of eMPA induces less epidermal cell death than dMPA.
Quantification and representative 3D reconstructed image of flank skin (~50 µm deep), 20x magnification, images of skin stained for viable/live (green) and non-viable/dead (pink) cells taken at time points 0 h, 24 h and 72 h after application of (A) 20 µl i.d. 31G, (B) eMPA and (C) dMPA, scale bar: 200 µm. (D) Quantification of dead cells in the epidermis at t = 0 h, n = 3 mice, mean ± SD.

<u>eMPA application induces LC migration but not dDC migration</u>

To assess whether the eMPA targeted specific resident APCs in the flank skin, we excised inguinal dLNs at t = 24, 48 and 72 h after eMPA or dMPA application (with PBS-based or OVA-based coating). During this time-frame (in naïve mice), DCs are only expected to migrate out of the skin in response to the MPA application based on previous reports on DCs in skin after MPA application [56-58]. Therefore, DC re-population of the skin after application was not assessed. Multi-colour flow cytometry was used to identify distinct DC subsets, including 'total DC' which subsets to resident DC, 'Res DC' or migratory DC 'Mig DC'. Mig DC further subsets to migratory LC 'Mig LC' or migratory dDC 'Mig dDC' (see Figure 7A for the gating strategy). These populations were defined by: total DCs (CD11c+ MHC II(lo/hi)) cells that were subdivided using mean florescent intensity (MFI) histograms into Res DC (CD11c+ MHC II (lo)) and Mig DC (CD11c+ MHC II (hi)). Mig DCs were then further sub-populated to Mig LCs (CD11c+ MHC II (hi) CD11b+ EpCAM+) and Mig dDCs (CD11c+ MHC II (hi) CD11b+ EpCAM(lo)).

Compared to dLNs from naïve mice, there were no significant differences between the numbers of live, single cells in any condition (SUPP 7). Concurrently, within each application group, there was no difference between total number of cells between time points t = 24, 48 or 72 h, nor between delivery of PBS or OVA within the Mig LC population nor within the Mig dDC population (SUPP 7). We henceforth compared eMPA and dMPA by combining data from all three time points and both formulations (PBS and OVA, n = 18). The total number of DCs between naïve, eMPA and dMPA was similar ($p = 0.57$) (SUPP 8), while the dMPA-treated dLNs demonstrated the presence of more Mig DCs, although not significantly ($p = 0.053$) (SUPP 8). Expression levels (MFI) of MHC II were significantly higher on the dMPA Mig DCs (naïve $p = 0.0008$, eMPA $p < 0.0001$) than the eMPA Mig DCs ($p = 0.0003$) (Figure 7B, right). Conversely, the eMPA dLNs contained more Res DCs than both the naïve ($p < 0.0001$) and dMPA ($p < 0.0001$) (SUPP 8). Both eMPA Res DCs

(Figure 7B, left) and Mig DCs (Figure 7B, right) expressed lower levels of MHC II than respective dMPA populations ($p < 0.0001$). Overall, the eMPA and dMPA induced LC migration while only the dMPA resulted in dDC migration (Figure 7C and D). Compared to naïve, the eMPA increased Mig LCs (number $p < 0.0001$, percent $p = 0.0003$) slightly more than the dMPA (number $p = 0.0004$, percent $p = 0.0016$), although this was not significant between the two MPAs ($p = 0.83$). While, the dMPA induced significantly more Mig dDCs than the eMPA (number $p = 0.0014$, percent $p < 0.0001$). Therefore, the eMPA preferentially targeted LCs while the dMPA targeted both LCs and dDCs.

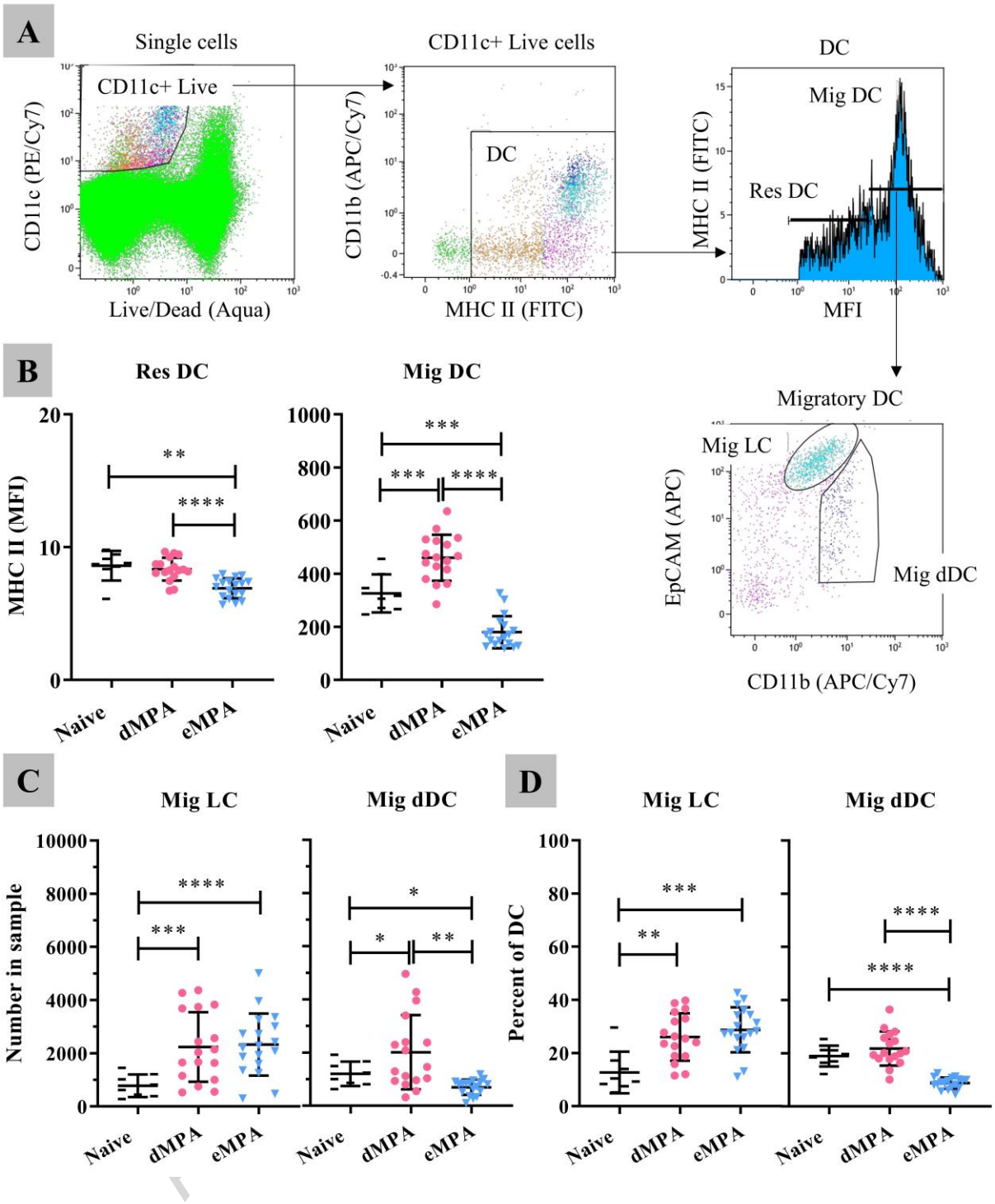

Figure 7: eMPAs result in specific migration of epidermal LCs. Quantification of migratory LCs and dDCs in inguinal dLN from combined time points and antigen conditions of either eMPA (▼) or dMPA (●) applications compared to naïve (-) mice. (A) Gating strategy to identify and quantify cell populations. (B) Graphs of the Mean Fluorescence Intensity (MFI) of MHC II for Res DC (left) and Mig DC (right). (C) Total number of Mig LC (left) and Mig dDC (right) cell populations. (D) Percent of Mig LC (left) and Mig dDC

(right) cell populations from DC population. MPA groups included n = 9 mice with n = 18 dLNs per group; naïve group n = 4 mice (n = 8 dLN). Graph: mean ± SD.

Discussion

This is first reported study (to our knowledge) of the rapid delivery of biomolecules targeted to viable epidermis of mice, whilst maintaining a low local inflammatory response. In achieving this, our findings open up exploration of the capabilities of the mouse model for therapies that would benefit from low inflammatory LC targeting such as asthma, AIT and chronic obstructive pulmonary disease. The study used polycarbonate MPAs, which is an inexpensive material that is well tolerated well by the skin's immunity [59]. Thus, a polycarbonate eMPA is a suitable candidate for repetitive, immune downregulating therapies such as AIT. We have shown that blunt-tipped eMPA designs deliver OVA antigen primarily to the epidermis of mouse flank skin, and preferentially induce LC migration. This is achieved with lower levels of skin inflammation than is induced by a dMPA. Additionally, Cohn et al. [24] showed that patient compliance significantly increases if AIT treatment duration is less than 15 minutes [24-26]. As is consistent with MPA application times previously reported in the literature [60, 61], the eMPA delivered the desired dose (0.1 μg) of OVA within two minutes. Although coating methods used in this report were crude, leading to a low delivery efficiency (SUPP 1), using a more efficient coating method such as dip coating or inkjet coating would improve dose sparing effects of eMPA delivery to Langerhans cells [62, 63].

Conical-MPA and slit-MPA projections were designed and tested at a variety of set application energies. In agreement with previous work of the microneedle field [42, 44, 64, 65] , conical-MPAs were unable to deliver to the shallow mouse epidermis alone. For example, when Crichton et al. [44], used a similar application energy (26 mJ), the conical-MPA penetrated into the dermis of ear skin. Conversely, the slit-MPAs were initially reported to increase penetration depth into mouse skin [40]. Yet, using polycarbonate slit-MPAs with a larger (blunter) tip surface area (Figure 1F), led to reduced penetration into the skin that could be maintained at a lower application energy (Figure 3), thus generating less cell death (Figure 6) and ultimately less skin inflammation (Figure 4 and Figure 5). This study is the first to show MPAs can be re-designed to not only target the epidermis but also maintain low skin inflammation despite a relatively high-density (7,000 projection/cm^2). This approach builds upon insights into the viscoelasticity of the skin and the mechanical application of MPAs thereof [44, 66, 67].

The closest epidermal-targeted MPA design to the eMPA previously reported is by Crichton et al. [44], which delivered OVA to the epidermal-dermal junction of mouse skin when applied by hand. Crichton et al. investigated the same MPA applied using a spring applicator at a range of application energies that led to penetration from the epidermal-dermal junction into approximately one third into mouse dermis. Interestingly, when application energy decreased, anti-OVA IgG response decreased (now known to be Th2-biased from unpublished data). Suggesting that lower application energies are necessary to avoid immune-activating responses. Additionally, Depelsenaire et al. reported that by halving the number of dMPA projections per MPA (from 3360 to 1600) induced a significantly lower titre of anti-Fluvax IgG after delivery of influenza vaccine [33]. This indicates that MPA surface area applied to the skin can correlate with the level of immune activation. This avenue of changing the MPA design and application conditions to alter specific immunity is yet to be explored systematically. Together, these studies suggest that the combination of decreased application energy and delivery surface area (i.e. $mm^2 \times mJ$) would also lead to a reduced immune-activating response. The eMPA has a significantly lower $mm^2 \times mJ$ than the dMPA, supporting its suitability to avoid the induction of immune-activating responses.

The LCs of the skin are well known to elicit either an antigen-specific immune regulation (e.g. Treg) [68, 69] or immune activation (e.g. Th1/Th2) [22, 70], however, the inflammatory threshold for LC-induced immune activation is yet to be determined. The eMPA defined here induces less skin inflammation than the dMPA, primarily penetrating into the epidermis, resulting in strata-specific APC migration (Figure 7). In comparison to more inflammatory (erythema present > 24 h) mouse epidermal-based delivery devices tested for AIT, such as ablative micro-fractional laser, OVA only administration increased allergic responses (Th2) and so additional Th1 adjuvants were required to prevent Th2 activation [71, 72]. While, delivery methods with low associated inflammatory responses, such as Viaskin®, enhanced Treg responses and prevented specific-Th2 activation in challenged mice [73, 74]. Although Viaskin® has shown great promise in AIT [31] by targeting delivery to the epidermis [15], each application repeat still takes 48 hours [75]. Even though T cell responses are still to be investigated for the eMPA, we hypothesis that the eMPA would preferentially activate tolerance similar to Viaskin®.

While delivery into the epidermis was achieved, it was also important in this study to assess that potential therapies would be taken up by the resident LCs and presented in the skin

dLNs. Here, we have shown that the eMPA specifically activated only LC migration while dMPA activated both LC and dDC migration (Figure 7). Interestingly, despite only inducing half the number of dead cells in the epidermis (Figure 6D), the eMPA dLNs contained the same number of migrating LCs (Mig LCs) as the dMPA. This is supported by Fernando et al. [76] who predicted that a dMPA of 16 mm^2 (as used here) would target therapeutic to approximately 2000 out of the 10,000 LCs available to migrate in mouse skin. It is possible that here, we have highlighted that there is a localised threshold of number of dead cells required to activate LC migration. So, even though the eMPA killed the lowest number of cells (relative to the dMPA and Fernando's dMPA), the number of dead cells killed by the eMPA is likely to still be above the minimal threshold to activate the same ratio of LCs as higher levels of cell death. This, however, does not address the maturation state of the migrated LC. Nakano (2012) [77] reported higher MHC II expression on DCs is required for Th2 priming in mice (and rats [78]) and correlates with an increase in Th1 activation. Therefore, because the expression of MHC II on Mig DC after eMPA was significantly lower than the Mig DCs of the dMPA (Figure 7B), the dMPA Mig DCs are significantly more likely to prime for effector T cell responses than the eMPA. Based on previous reports of MPAs similar to the dMPA, Ng et al. [79] found high-density dMPAs preferentially activated CD8+ T cells, while Shakya et al. [80] found low-density dMPAs induced a Th1-skewed response. Additionally, the eMPA dLNs contained a higher ratio of Res DCs than the dMPA similar to ratios seen in Viaskin® application, a device that has several promising results in AIT [15]. We hypothesise that, as the eMPA does not activate dDC migration nor high levels of skin inflammation, it is less likely to activate immunity like the dMPAs and is more likely to deliver antigen to the LCs for specific tolerance. To test this, eMPAs should be investigated in future mouse model experiments of low inflammatory LC targeted immunotherapies such as asthma, AIT and chronic obstructive pulmonary disease.

Conclusion

Here, we describe an MPA specifically targeting the epidermal layer of skin in mice – the eMPA. The eMPA caused a lower level of skin inflammation response relative to a dMPA. To achieve this, the eMPA was designed to have a high-density of blunt tipped projections which was applied with a low energy. Additionally, the eMPA device can specifically target the LCs of the skin without activating dDC. Due to the specific cell targeting, eMPAs could lead to higher therapy efficiency using lower doses (i.e. making them safer and cheaper), increasing availability of the treatment and patient compliance. Therefore, this device

provides a valuable tool for the necessary studies to advance LC targeting with a practical device from pre-clinical tests in mice to epidermal-based therapies in patients.

Acknowledgements

We would like to acknowledge the AIBN animal house facility staff, particularly Barb Arnts, Simon Webster and Telischa Parfitt for care and maintenance of the mice used here. The Australian National Fabrication Facility – Queensland node for silicon wafer manufacture. The Centre for Microscopy and Microanalysis for use of the facility. Rob Sullivan of the Histology department (Queensland Brain Institute) for paraffin processing and use of the facility. The Flow Core Facility (TRI) for use of the facility. Finally, Jonathan Wei and Hong Nick Lee for reading drafts of the manuscripts.

Funding

This work is supported by the Australian Research Council Centre of Excellence in Convergent Bio-Nano Science & Technology Grant (CE140100036).

References

[1] Smarr, C.B., P.J. Bryce, and S.D. Miller, *Antigen-Specific Tolerance in Immunotherapy of Th2-Associated Allergic Diseases.* Critical reviews in immunology, 2013. **33**(5): p. 389-414.

[2] Vroman, H., R.W. Hendriks, and M. Kool, *Dendritic Cell Subsets in Asthma: Impaired Tolerance or Exaggerated Inflammation?* Frontiers in Immunology, 2017. **8**.

[3] Tsoumakidou, M., et al., *Tolerogenic signaling by pulmonary CD1c+ dendritic cells induces regulatory T cells in patients with chronic obstructive pulmonary disease by IL-27/IL-10/inducible costimulator ligand.* J Allergy Clin Immunol, 2014. **134**(4): p. 944-954.e8.

[4] Kleijwegt, F.S., et al., *Tolerogenic dendritic cells impede priming of naive CD8(+) T cells and deplete memory CD8(+) T cells.* Eur J Immunol, 2013. **43**(1): p. 85-92.

[5] Mutyambizi, K., C.L. Berger, and R.L. Edelson, *The balance between immunity and tolerance: The role of Langerhans cells.* Cellular and molecular life sciences : CMLS, 2009. **66**(5): p. 831-840.

[6] Shklovskaya, E., et al., *Langerhans cells are precommitted to immune tolerance induction.* Proceedings of the National Academy of Sciences of the United States of America, 2011. **108**(44): p. 18049-18054.

[7] Sen, D., et al., *Selective and site-specific mobilization of dermal dendritic cells and Langerhans cells by Th1-and Th2-polarizing adjuvants.* Proceedings of the National Academy of Sciences of the United States of America, 2010. **107**(18): p. 8334-8339.

[8] de Aguero, M.G., et al., *Langerhans cells protect from allergic contact dermatitis in mice by tolerizing CD8(+) T cells and activating Foxp3(+) regulatory T cells.* Journal of Clinical Investigation, 2012. **122**(5): p. 1700-1711.

[9] Seneschal, J., et al., *Human epidermal Langerhans cells maintain immune homeostasis in skin by activating skin resident regulatory T cells.* Immunity, 2012. **36**(5): p. 873-884.

[10] Stary, G., et al., *Glucocorticosteroids modify Langerhans cells to produce TGF-beta and expand regulatory T cells.* J Immunol, 2011. **186**(1): p. 103-112.

[11] Holzmann, S., et al., *A Model System Using Tape Stripping for Characterization of Langerhans Cell-Precursors In Vivo.* J Invest Dermatol, 2004. **122**(5): p. 1165-1174.

[12] Mondoulet, L., et al., *Intact skin and not stripped skin is crucial for the safety and efficacy of peanut epicutaneous immunotherapy (EPIT) in mice.* Clin Transl Allergy, 2012. **2**(22).

[13] Senti, G., S. von Moos, and T.M. Kündig, *Epicutaneous allergen administration: is this the future of allergen-specific immunotherapy?* Allergy, 2011. **66**(6): p. 798-809.

[14] Callard, R.E. and J.I. Harper, *The skin barrier, atopic dermatitis and allergy: a role for Langerhans cells?* Trends in Immunology, 2007. **28**(7): p. 294-298.

[15] Dioszeghy, V., et al., *Epicutaneous immunotherapy results in rapid allergen uptake by dendritic cells through intact skin and downregulates the allergen-specific response in sensitized mice.* J Immunol, 2011. **186**(10): p. 5629-5637.

[16] Tong, P.L., et al., *The Skin Immune Atlas: Three-Dimensional Analysis of Cutaneous Leukocyte Subsets by Multiphoton Microscopy.* J Invest Dermatol, 2015. **135**(1): p. 84-93.

[17] Wei, J.C.J., et al., *Space- and time-resolved investigation on diffusion kinetics of human skin following macromolecule delivery by microneedle arrays.* Scientific Reports, 2018. **8**.

[18] Herkenne, C., et al., *In Vivo Methods for the Assessment of Topical Drug Bioavailability.* Pharmaceutical Research, 2008. **25**(1): p. 87-103.

[19] Ding, Z., et al., *Microneedle arrays for the transcutaneous immunization of diphtheria and influenza in BALB/c mice.* J Control Release, 2009. **136**(1): p. 71-78.

[20] Jain, A., et al., *Novel strategies for effective transdermal drug delivery: a review.* Crit Rev Ther Drug Carrier Syst, 2014. **31**(3): p. 219-272.

[21] Fluhr, J.W., K.R. Feingold, and P.M. Elias, *Transepidermal water loss reflects permeability barrier status: validation in human and rodent in vivo and ex vivo models.* Exp Dermatol, 2006. **15**(7): p. 483-492.

[22] Oyoshi, M.K., et al., *Mechanical injury polarizes skin dendritic cells to elicit a Th2 response by inducing cutaneous TSLP expression.* J Allergy Clin Immunol, 2010. **126**(5): p. 976-984.e5.

[23] Larrañeta, E., et al., *Microneedle arrays as transdermal and intradermal drug delivery systems: Materials science, manufacture and commercial development.* Materials Science and Engineering: R: Reports, 2016. **104**: p. 1-32.

[24] Cohn, J.R. and A. Pizzi, *Determinants of patient compliance with allergen immunotherapy.* J Allergy Clin Immunol, 1993. **91**(3): p. 734-737.

[25] More, D.R. and L.L. Hagan, *Factors affecting compliance with allergen immunotherapy at a military medical center.* Ann Allergy Asthma Immunol, 2002. **88**(4): p. 391-394.

[26] Jin, J.-f., et al., *The optimal choice of medication administration route regarding intravenous, intramuscular, and subcutaneous injection.* Patient preference and adherence, 2015. **9**: p. 923-942.

[27] Kendall, M., et al., *Downregulation of IgE antibody and allergic responses in the lung by epidermal biolistic microparticle delivery.* J Allergy Clin Immunol, 2006. **117**(2): p. 275-282.

[28] Oberli, M.A., et al., *Ultrasound-enhanced transdermal delivery: recent advances and future challenges.* Therapeutic delivery, 2014. **5**(7): p. 843-857.

[29] Chen, X., et al., *Micro-fractional epidermal powder delivery for improved skin vaccination.* J Control Release, 2014. **192**: p. 310-316.

[30] Raju, P.A., et al., *Assessment of epidermal cell viability by near infrared multi-photon microscopy following ballistic delivery of gold micro-particles.* Vaccine, 2006. **24**(21): p. 4644-4647.

[31] Mondoulet, L., et al., *Epicutaneous immunotherapy on intact skin using a new delivery system in a murine model of allergy.* Clin Exp Allergy, 2010. **40**(4): p. 659-667.

[32] Norman, J.J., et al., *Microneedle patches: Usability and acceptability for self-vaccination against influenza.* Vaccine, 2014. **32**(16): p. 1856-1862.

[33] Depelsenaire, A.C., et al., *Colocalization of cell death with antigen deposition in skin enhances vaccine immunogenicity.* J Invest Dermatol, 2014. **134**(9): p. 2361-2370.

[34] Griffin, P., et al., *Safety, acceptability and tolerability of uncoated and excipient-coated high density silicon micro-projection array patches in human subjects.* Vaccine, 2017. **35**: p. 6676-6684.

[35] Kim, Y.C., et al., *Improved influenza vaccination in the skin using vaccine coated microneedles.* Vaccine, 2009. **27**(49): p. 6932-6938.

[36] Coffey, J.W., S.R. Corrie, and M.A. Kendall, *Early circulating biomarker detection using a wearable microprojection array skin patch.* Biomaterials, 2013. **34**(37): p. 9572-9583.

[37] Bhatnagar, S., K. Dave, and V.V.K. Venuganti, *Microneedles in the clinic.* Journal of Controlled Release, 2017. **260**: p. 164-182.

[38] Mondoulet, L., et al., *Epicutaneous immunotherapy using a new epicutaneous delivery system in mice sensitized to peanuts.* Int Arch Allergy Immunol, 2011. **154**(4): p. 299-309.

[39] Yeow, B., et al., *Surface Modification and Characterization of Polycarbonate Microdevices for Capture of Circulating Biomarkers, Both in Vitro and in Vivo.* Analytical Chemistry, 2013. **85**(21): p. 10196-10204.

[40] Crichton, M.L., et al., *The changing shape of vaccination: improving immune responses through geometrical variations of a microdevice for immunization.* Sci Rep, 2016. **6**: p. 27217.

[41] Fernando, G.J., et al., *Nanopatch targeted delivery of both antigen and adjuvant to skin synergistically drives enhanced antibody responses.* J Control Release, 2012. **159**(2): p. 215-221.

[42] Chen, X., et al., *Site-Selectively Coated, Densely-Packed Microprojection Array Patches for Targeted Delivery of Vaccines to Skin.* Advanced Functional Materials, 2011. **21**(3): p. 464-473.

[43] Coffey, J.W., et al., *Dynamic application of microprojection arrays to skin induces circulating protein extravasation for enhanced biomarker capture and detection.* Biomaterials, 2016. **84**: p. 130-143.

[44] Crichton, M.L., et al., *The effect of strain rate on the precision of penetration of short densely-packed microprojection array patches coated with vaccine.* Biomaterials, 2010. **31**(16): p. 4562-4572.

[45] Raphael, A.P., et al., *Targeted, needle-free vaccinations in skin using multilayered, densely-packed dissolving microprojection arrays.* Small, 2010. **6**(16): p. 1785-1793.

[46] Draize, J.H., G. Woodard, and H.O. Calvery, *Methods for the study of irritation and toxicity of substances applied topically to the skin and mucous membranes.* J Pharm Exper Therap, 1944. **82**(3): p. 377.

[47] Pasetti, M.F., et al., *An improved Francisella tularensis Live Vaccine Strain (LVS) is well tolerated and highly immunogenic when administered to rabbits in escalating doses using various immunization routes.* Vaccine, 2008. **26**(14): p. 1773-1785.

[48] Kool, M., et al., *Alum adjuvant boosts adaptive immunity by inducing uric acid and activating inflammatory dendritic cells.* J Exp Med, 2008. **205**(4): p. 869-882.

[49] Chandra, J., et al., *Batf3 selectively determines acquisition of CD8+ dendritic cell phenotype and function.* Immunology and cell biology, 2017. **95**(2): p. 215-223.

[50] Egekvist, H., P. Bjerring, and L. Arendt-Nielsen, *Pain and mechanical injury of human skin following needle insertions.* European Journal of Pain, 1999. **3**(1): p. 41-49.

[51] Gopee, N.V., et al., *Response of mouse skin to tattooing: use of SKH-1 mice as a surrogate model for human tattooing.* Toxicol Appl Pharmacol, 2005. **209**(2): p. 145-158.

[52] Rock, K.L., J.J. Lai, and H. Kono, *Innate and adaptive immune responses to cell death.* Immunol Rev, 2011. **243**(1): p. 191-205.

[53] Thompson, C.B., *Apoptosis in the pathogenesis and treatment of disease.(Cover Story).* Science, 1995. **267**(5203): p. 1456-1462.

[54] Green, D.R., et al., *Immunogenic and tolerogenic cell death.* Nat Rev Immunol, 2009. **9**(5): p. 353-363.

[55] Pasparakis, M., I. Haase, and F.O. Nestle, *Mechanisms regulating skin immunity and inflammation.* Nat Rev Immunol, 2014. **14**(5): p. 289-301.

[56] Pearton, M., et al., *Influenza virus-like particles coated onto microneedles can elicit stimulatory effects on Langerhans cells in human skin.* Vaccine, 2010. **28**(37): p. 6104-6113.

[57] Ruutu, M.P., et al., *Increasing mechanical stimulus induces migration of Langerhans cells and impairs the immune response to intracutaneously delivered antigen.* Exp Dermatol, 2011. **20**(6): p. 534-536.

[58] Rattanapak, T., et al., *Dynamic visualization of dendritic cell-antigen interactions in the skin following transcutaneous immunization.* PLoS One, 2014. **9**(2): p. e89503.

[59] Jin, C.Y., et al., *Mass producible and biocompatible microneedle patch and functional verification of its usefulness for transdermal drug delivery.* Biomedical Microdevices, 2009. **11**(6): p. 1195-1203.

[60] Donnelly, R.F., T.R. Raj Singh, and A.D. Woolfson, *Microneedle-based drug delivery systems: Microfabrication, drug delivery, and safety.* Drug delivery, 2010. **17**(4): p. 187-207.

[61] Kwon, K.M., et al., *Microneedles: quick and easy delivery methods of vaccines.* Clinical and Experimental Vaccine Research, 2017. **6**(2): p. 156-159.

[62] Shakya, A.K., C.H. Lee, and H.S. Gill, *Cutaneous vaccination with coated microneedles prevents development of airway allergy.* Journal of Controlled Release, 2017.

[63] O'Mahony, C., et al., *Accuracy and feasibility of piezoelectric inkjet coating technology for applications in microneedle-based transdermal delivery.* Microelectronic Engineering, 2017. **172**: p. 19-25.

[64] Kim, Y.-C. and M.R. Prausnitz, *Enabling skin vaccination using new delivery technologies.* Curr Top Microbiol Immunol, 2012. **351**: p. 77-112.

[65] Carey, J.B., et al., *Microneedle array design determines the induction of protective memory CD8+ T cell responses induced by a recombinant live malaria vaccine in mice.* PLoS One, 2011. **6**(7): p. e22442.

[66] Kendall, M.A.F., Y.-F. Chong, and A. Cock, *The mechanical properties of the skin epidermis in relation to targeted gene and drug delivery.* Biomaterials, 2007. **28**(33): p. 4968-4977.

[67] Crichton, M.L., et al., *Elastic modulus and viscoelastic properties of full thickness skin characterised at micro scales.* Biomaterials, 2013. **34**(8): p. 2087-2097.

[68] Balmert, S.C., et al., *In vivo induction of regulatory T cells promotes allergen tolerance and suppresses allergic contact dermatitis.* J Control Release, 2017. **261**: p. 223-233.

[69] Yoshiki, R., et al., *IL-10-producing Langerhans cells and regulatory T cells are responsible for depressed contact hypersensitivity in grafted skin.* J Invest Dermatol, 2009. **129**(3): p. 705-713.

[70] Yasuda, T., et al., *Intradermal Delivery of Antigens Enhances Specific IgG and Diminishes IgE Production: Potential Use for Vaccination and Allergy Immunotherapy.* PLoS ONE, 2016. **11**(12): p. e0167952.

[71] Weiss, R., et al., *Transcutaneous vaccination via laser microporation.* Journal of controlled release : official journal of the Controlled Release Society, 2012. **162**(2): p. 391-399.

[72] Kumar, M.N., C. Zhou, and M.X. Wu, *Laser-Facilitated Epicutaneous Immunotherapy to IgE-Mediated Allergy.* J Control Release, 2016. **235**: p. 82-90.

[73] Dioszeghy, V., et al., *The regulatory T cells induction by epicutaneous immunotherapy is sustained and mediates long-term protection from eosinophilic disorders in peanut-sensitized mice.* Clin Exp Allergy, 2014. **44**(6): p. 867-881.

[74] Tordesillas, L., et al., *Epicutaneous immunotherapy induces gastrointestinal LAP+ regulatory T cells and prevents food-induced anaphylaxis.* J Allergy Clin Immunol, 2016. **139**: p. 189-201.e4.

[75] Dioszeghy, V., et al., *Differences in phenotype, homing properties and suppressive activities of regulatory T cells induced by epicutaneous, oral or sublingual immunotherapy in mice sensitized to peanut.* Cell Mol Immunol, 2017. **14**(9): p. 770-782.

[76] Fernando, G.J., et al., *Potent immunity to low doses of influenza vaccine by probabilistic guided micro-targeted skin delivery in a mouse model.* PLoS One, 2010. **5**(4): p. e10266.

[77] Nakano, H., et al., *Pulmonary CD103(+) dendritic cells prime Th2 responses to inhaled allergens.* Mucosal immunology, 2012. **5**(1): p. 53-65.

[78] Leffler, J., et al., *Functional differences in airway dendritic cells determine susceptibility to IgE-sensitization.* Immunol Cell Biol, 2018. **96**(3): p. 316-329.

[79] Ng, H.I., G.J. Fernando, and M.A. Kendall, *Induction of potent CD8(+) T cell responses through the delivery of subunit protein vaccines to skin antigen-presenting cells using densely packed microprojection arrays.* J Control Release, 2012. **162**(3): p. 477-484.

[80] Shakya, A.K. and H.S. Gill, *A comparative study of microneedle-based cutaneous immunization with other conventional routes to assess feasibility of microneedles for allergy immunotherapy.* Vaccine, 2015. **33**(33): p. 4060-4064.

HIGHLIGHTS

- First microprojection array to deliver primarily to the epidermis of mouse skin.
- The eMPA rapidly delivered ovalbumin with a low skin inflammation response.
- The eMPA preferentially promotes Langerhans cell migration out of skin.